PHOTON BACKGROUNDS AT THE CLIC INTERACTION POINT DUE TO LOSSES IN THE POST-COLLISION EXTRACTION LINE

M. D. Salt*, R. B. Appleby, The Cockcroft Institute, Warrington, United Kingdom
K. Elsener, CERN, Geneva, Switzerland
A. Ferrari, Uppsala University, Sweden

Abstract

The CLIC beam delivery system focuses 1.5 TeV electron and positron beams to a nanometre-sized cross section when colliding them at the interaction point (IP). The intense focusing leads to large beam-beam effects, causing the production of beamstrahlung photons, coherent and incoherent e^+e^- pairs, as well as a significant disruption of the main beam. The transport of the post-collision beams requires a minimal loss extraction line, with high acceptance for energy deviation and divergence. The current design includes vertical bends close to the IP in order to separate the charged particles with a sign opposite to the main beam into a diagnostic-equipped intermediate dump, whilst transporting the photons and the main beam to the final dump. Photon and charged particle losses on magnet masks and dumps result in a complex radiation field and IP background particle fluxes. In this paper, the electromagnetic backgrounds at the IP arising from the losses occurring closest to the collision point are calculated.

CLIC EXTRACTION LINE DESIGN

The conceptual design of the 150 m long CLIC extraction line from the IP to the final dump is described in [1]. A side view of the layout is shown in Figure 1.
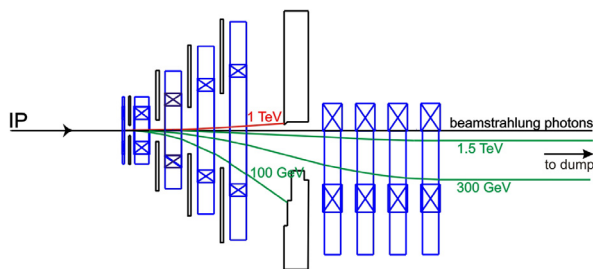

Figure 1: Layout of the CLIC extraction line.

The first part of the line is a vertical bending region designed to separate the disrupted beam, the beamstrahlung photons and the coherent pairs. In a second part, the disrupted beam, together with the high-energy component of the same-charge coherent pair particles, are bent back into a parallel beam, which is then transported to the final dump, together with the beamstrahlung photons. The lower energy component of the main beam and of the same-charge coherent pair particles, as well as all particles with the opposite charge, are directed onto an intermediate dump. The

bending region consists of five window frame magnets with a field strength of 0.8 T. The first magnet, designed to deflect only the lowest energy particles, is 0.5 m long. The second magnet has a length of 3.5 m, the following three magnets are 4.0 m long. Dispersion effects in the magnets further increase the vertical beam size, in particular due to the lower energy component of the outgoing charged beams. To prevent damage to the magnets, a set of graphite masks are inserted to absorb the tails of the particle distribution. The back-bending region consists of four identical C-type magnets. Since the intermediate dump is designed to absorb all the lower energy particles, no collimation is needed in the back-bending region.

BACKSCATTERED PHOTONS

Electrons and positrons incident on the masks interact within the material via a number of physical processes. Initially, these lost particles may be considered to be of high-energy (at least a few GeV), which form electromagnetic cascades of bremsstrahlung photons and e^+e^- pairs. The resultant showering permits angular deflections such that the forward moving lepton may generate photons and pair-produced particles even in the backwards direction, towards the interaction point. As these showers develop, the particles produced eventually reach the low-energy range where electrons primarily lose energy via ionization, and photons via the photoelectric effect, Compton scattering and Rayleigh scattering. Multiple scattering through small angles may lead to these particles being directed towards the IP, contributing to the photon background. Of these processes, Compton scattering is the most dominant, producing photons at the IP in the 100 - 200 keV energy range.

Photon Background Calculation

In order to calculate the photon flux at the IP due to losses in the extraction line, it is necessary to track the outgoing beam particles, model any interaction within material and then track the resulting particles back to the IP, following a similar method as in [2]. The outgoing beam samples used for this study were produced with the beam-beam simulator Guinea-Pig [3]. The electromagnetic physics simulation in GEANT4 [4] enables such a study, using the BDSIM toolkit [5] to generate the accelerator-based modelling.

---

* Michael.Salt@hep.manchester.ac.uk

FIRST MAGNETS AND MASK

The mask between the first magnet (0.5 m long) and the second magnet (3.5 m long) has been identified as a dominant source of IP photons. This is due to two main reasons.

- Photon flux density decays rapidly with increasing distance from the source in free space. At only 29.0 m from the IP, the first mask is the closest major source of photons. There are losses in the first 0.5 m magnet, but these are three orders of magnitude lower than in the mask.
- In order to concentrate beam losses in the masks, rather than in the magnets, the vertical aperture of the mask is designed to be much smaller than the aperture of the first magnet, as shown in Figure 2. There is a direct line of sight from the material of the mask to the IP. Due to the curved trajectory of the outgoing beams, other masks do not have such a line of sight because other elements upstream shield the IP.
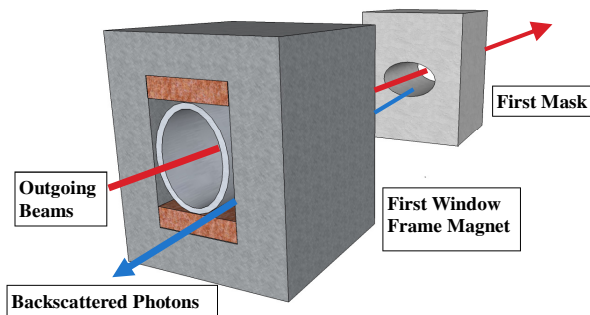

Figure 2: Schematic view of the first magnet and first mask simulated in this study.

This mask is 0.5 m long, and modelled as a graphite box with transverse dimensions of 0.5 m × 1.0 m. The aperture is an ellipse with a full-width cross section of 200 mm × 132 mm.

Backscattered Photons from the Mask

There are no losses from the disrupted beam and the same-charge particles of the coherent pairs on the first mask. The interactions of the particles with an opposite charge with the graphite cause an elliptical photon shadow of the mask aperture. Figure 3 shows the corresponding x and y distributions. Some photons pass through the entire body of the graphite and escape the volume to give a non-zero photon density outside of the 0.5 m × 1.0 m box. In the horizontal distribution, at the outer edges of the graphite mask (0.25 m), a lower density is observed. This is due to the shielding effect, preventing photons from traversing in this direction. The vertical distribution in Figure 3 shows a slight asymmetry, consistent with the fact that the particles of opposite charge to the main beam are deflected upwards and are, therefore, predominantly lost in the upper

half of the mask. Figure 4 shows that the angular distributions of photons exiting the mask in the direction of the IP are quasi-isotropic. Figure 5 shows the energy distribution of backscattered on-axis photons exiting the mask. Only about 1 in 10000 backscattered photons have an energy above 1 MeV.
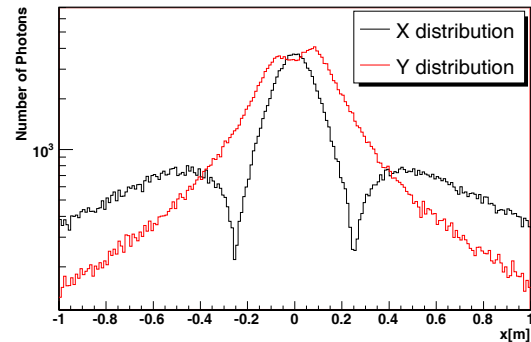

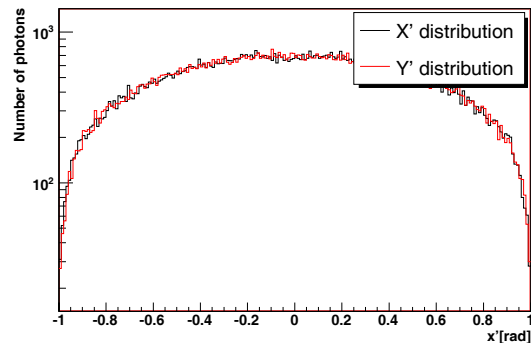Figure 3: Backscattered photon distribution at the entrance of the mask (s = 29.0 m) as viewed from IP.

Figure 4: Angular distribution of backscattered photons at the entrance of the mask (s = 29.0 m).
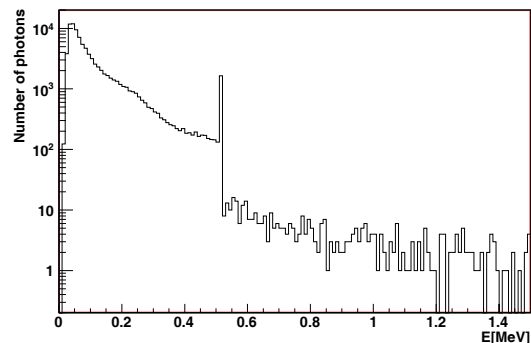

Figure 5: Backscattered on-axis photon energy spectrum at the entrance of the mask (s = 29.0 m).

The Masking Effect of the First Magnet

The primary purpose of the first magnet is to create a small dispersion such that very low energy particles can

be removed by the first mask, to prevent excessive losses in the second magnet. In addition, the magnet acts as a mask to backscattered photons. The first magnet has external iron flux return dimensions of 494 mm × 976 mm with a rectangular aperture of 222 mm × 450 mm. The beam travels in an elliptical beam pipe with full-width apertures of 200 mm × 440 mm.

Figure 6 shows a distinct area of low photon density in the region of the iron flux return and copper coils. This is due to the shielding effect of the iron. Outside this region, photons with large x' and y' bypass the magnet, but line of sight arguments suggest that these will not be incident on the IP. In the centre, there are four very high-density regions, which represent the four air-gaps between the rectangular magnet aperture and the elliptical beam pipe. There is also a high density of photons in the vacuum vessel, which are likely to contribute to IP backgrounds. Figure 7 shows the angular distributions of photons exiting the upstream face of the first magnet. In Figure 8, the energy spectrum of these photons is shown.
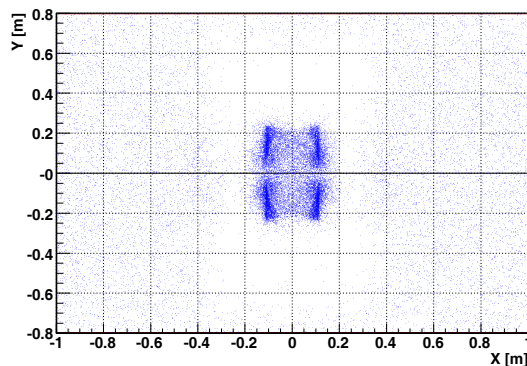

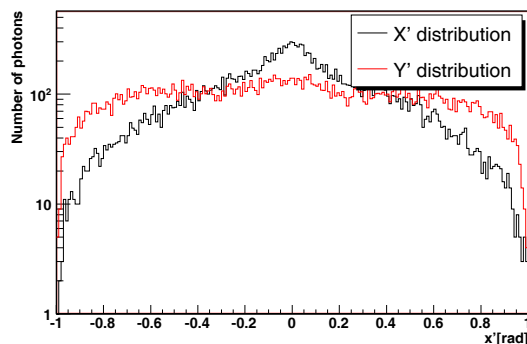Figure 6: Backscattered photons at the entrance of the first magnet (s = 27.5 m) as viewed from IP.

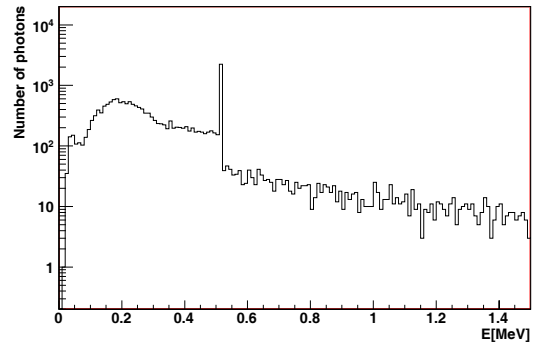Figure 7: Angular distribution of backscattered photons at the entrance of the first magnet (s = 27.5 m).

Figure 8: Backscattered on-axis photon energy spectrum at the entrance of the first magnet (s = 27.5 m).

Photons at the IP

By extrapolation of the positions and angles of the photons at s = 27.5 m, it is possible to calculate the projected flux at the IP. Using the simplified model in Figure 2, with the conservative assumption that there is no absorbing material between the IP and the first magnet, the on-axis flux at s = 0.0 m is 0.727 ± 0.048 cm^{-2} per bunch crossing, or 11300 ± 740 cm^{-2}s^{-1}.

SUMMARY AND OUTLOOK

The investigation of backgrounds at the CLIC IP due to losses in the extraction line has started with the study of backscattered photons due to particle losses at the first mask, at s = 29.0 m from the IP. This mask is likely the most important source of background photons from the extraction line. In a first simplified GEANT analysis, less than one background photon per bunch crossing is found to reach the IP. In a next step, additional magnets and masks, as well as the intermediate and final dumps of the extraction line will be added. Approximate models of vacuum tubes, final focusing quadrupoles and forward calorimeters will be introduced in the region between the IP and the first magnet (s = 27.5 m). At a later stage, backscattering of neutrons from the extraction line will also be investigated.

REFERENCES

[1] A. Ferrari et. al., *Conceptual design of a beam line for post-collision extraction and diagnostics at the multi-TeV Compact Linear Collider*, PRST-AB 12, 021001 (2009).

[2] O. Dadoun, P. Bambade, *Backscattering of Secondary Particles into the ILC Detectors from Beam Losses Along the Extraction Lines*, EUROTeV-Report-2007-047.

[3] D. Schulte, *Ph.D Thesis*, University of Hamburg, 1996, TESLA 97-08.

[4] S. Agostinelli et. al., *GEANT4 - A Simulation Toolkit*, Nucl. Instrum. Methods A506 (2003) 250-303, http://geant4.CERN.ch.

[5] I. Agapov, G. Blair, J. Carter, O. Dadoun, *The BDSIM Toolkit*, EUROTeV-Report-2006-014-1.